APPARATUS AND DEMONSTRATION NOTES

Jeffrey S. Dunham, *Editor*

Department of Physics, Middlebury College, Middlebury, Vermont 05753

This department welcomes brief communications reporting new demonstrations, laboratory equipment, techniques, or materials of interest to teachers of physics. Notes on new applications of older apparatus, measurements supplementing data supplied by manufacturers, information which, while not new, is not generally known, procurement information, and news about apparatus under development may be suitable for publication in this section. Neither the *American Journal of Physics* nor the Editors assume responsibility for the correctness of the information presented. Submit materials to Jeffrey S. Dunham, *Editor*.

Mechanics of the slow draining of a large tank under gravity

Josué Njock Libii[a)]

Department of Engineering, Indiana University—Purdue University Fort Wayne, Fort Wayne, Indiana 46805-1499

I. INTRODUCTION

It has been our experience that students find mechanics fun and exciting when they are able to use what they have learned to model and to predict the behavior of familiar phenomena. For this reason, we have made considerable efforts to design experiments for the first course in fluid mechanics that are simple and easy to visualize, and that relate theoretical concepts from mechanics directly to the experience that students have with familiar phenomena. These experiments are particularly helpful when one has a class with students who are likely to get lost in the mathematical details that abound in the study of fluid flows. To illustrate this point, we present a draining experiment that is one of many laboratory exercises used to support the first course in fluid mechanics.

The experiment itself consists of draining a large cylindrical tank under the influence of gravity. The tank's axis of revolution is vertical; its top is open to the atmosphere, and it is drained through a small orifice located at the bottom of the tank. We measure both the total time it takes to drain the tank completely and the draining pattern itself, that is, how the volume of liquid in the tank changes with time during the draining process. We model the liquid as an incompressible and inviscid fluid and the flow as quasisteady and irrotational.

Although the actual flow is that of a viscous fluid, the observed behavior is compared with that predicted by the theory of the irrotational draining of an inviscid fluid. When the cross-sectional area of the exit orifice is much smaller than that of the tank, this comparison shows that the inviscid-fluid model approximates the behavior of the real fluid quite well. First, we describe the theory used for modeling, then the experiment itself. Finally, we show experimental results obtained and compare them to theory.

II. THEORY

Consider a cylindrical container of a circular cross section (the tank) that is oriented such that its axis of rotational symmetry is vertical. The tank is open to the atmosphere at the top so that water, or some other liquid, can be poured into the tank easily. The bottom of the tank is capped, but the cap has an orifice placed at its center through which liquid can drain. The tank is equipped with plugs that have openings of various diameters. The plugs can be threaded into the tank so as to change the diameter of the opening. Figure 1 shows the experimental setup.

Let A_t denote the inside cross-sectional area of the tank, A_0 the inside cross-sectional area of the opening of a plug, h_0 the initial elevation of the free surface relative to the bottom of the tank, h the instantaneous elevation of the free surface relative to the bottom of the tank at time t, t the time elapsed since the beginning of the draining process, t_d the total time needed to completely drain the tank of liquid, and g the local acceleration of gravity. Applying the unsteady conservation of energy for open systems to this problem results in the following equation that governs the variation with time of the instantaneous elevation of the free surface, $h(t)$, relative to the bottom of the tank:[1]

$$h\left(g + \frac{d^2h}{dt^2}\right) = \frac{1}{2}\left(\frac{dh}{dt}\right)^2\left[\left(\frac{A_t}{A_0}\right)^2 - 1\right]. \quad (1)$$

When the tank drains slowly, one can expect the acceleration of the free surface of the liquid to be very small compared to the acceleration of gravity. This means that $g \gg d^2h/dt^2$, and Eq. (1) then becomes

$$hg = \frac{1}{2}\left(\frac{dh}{dt}\right)^2\left[\left(\frac{A_t}{A_0}\right)^2 - 1\right]. \quad (2)$$

Equation (2) can now be integrated to obtain $h(t)$. When this is done, and the quantities involved are made dimensionless through scaling, one finds that the elevation of the free surface, h, varies with time according to[2]

$$\frac{h}{h_0} = \left(1 - \frac{t}{t_d}\right)^2, \quad (3a)$$
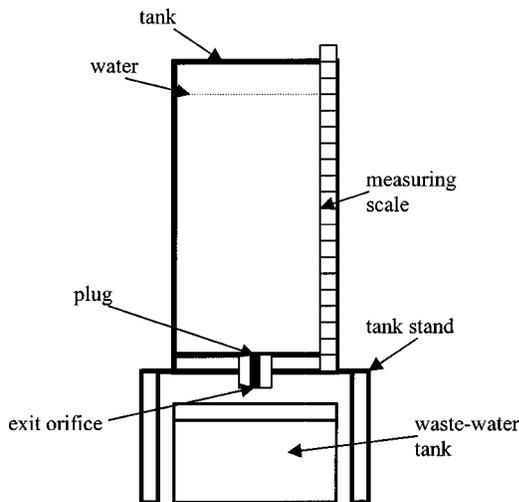
Fig. 1. Diagram of the experimental setup showing the orientation of the tank, the draining orifice fitted with a plug, and the tank stand.

and the velocity and acceleration of the free surface are given, respectively, by

$$\frac{dh}{dt} = -\frac{2h_0}{t_d}\left(1 - \frac{t}{t_d}\right) \tag{3b}$$

and

$$\frac{d^2h}{dt^2} = -\frac{2h_0}{t_d^2}, \tag{3c}$$

where the total time necessary to completely drain the tank, t_d, is given by

$$t_d = \left(\frac{2h_0}{g}\right)^{1/2}\left[\left(\frac{A_t}{A_0}\right)^2 - 1\right]^{1/2}. \tag{4}$$

This expression for t_d is reminiscent of the time it takes a free-falling particle to drop through a distance h_0 from rest. Indeed, for a particle that is released from rest at height h_0 above a reference level and falls freely in the absence of air resistance, the instantaneous elevation above that reference level, $h_p(t)$, and the duration of the fall, t_f, are given, respectively, by

$$\frac{h_p}{h_0} = 1 - \left(\frac{t}{t_f}\right)^2 \tag{5}$$

and

$$t_f = \sqrt{\frac{2h_0}{g}}. \tag{6}$$

The instantaneous velocity of the falling particle, $v_p(t)$, is given by

$$v_p(t) = -2\frac{h_0}{t_f}\left(\frac{t}{t_f}\right) \tag{7}$$

and

$$v_p(t_f) = -\sqrt{2gh_0}, \tag{8}$$

where t_f denotes the time it takes a particle to fall freely from rest under gravity from $h_p(0) = h_0$ to $h_p(t_f) = 0$, and v_f is the velocity achieved by the particle when $h_p = 0$. It is convenient to write the expression for t_d in Eq. (4) in a form that is similar to the expression for t_f in Eq. (6). Doing so leads to

$$t_d = \sqrt{\frac{2h_0}{g_m}}, \tag{9}$$

where

$$g_m = \frac{g}{[(A_t/A_0)^2 - 1]}. \tag{10}$$

The quantity g_m given in Eq. (10) can be considered to be the modified acceleration of gravity resulting from the constriction of the flow at the draining orifice. It indicates that the rate of descent of the free surface during draining will be slower than the velocity of freefall.

III. EXPERIMENT

We performed experiments to gather data that would allow us to compare theory to experiment. A cylindrical shell made of Plexiglas was used as the tank in this experiment. The shell is capped at its lower end to produce a transparent cylinder that can hold water. One or more orifices can be added to the cap. In our case, we used a single orifice but fabricated many threaded plugs. Holes of different diameters were drilled into the threaded plugs. By threading a drilled plug into the orifice, we could change the diameter of the exit orifice. A graduated scale was glued vertically along the length of the tank and it was used to track the position of the free surface of the water in the tank during the draining process. After selecting a given plug and threading it into the orifice, the tank was filled to a specified height and the water was allowed to come to rest. Then, the drain was opened and, using a stopwatch, we observed and recorded the location of the free surface as a function of time during draining. Once data were collected using one plug, the experiment was repeated using another plug. In this way, we collected data for different plugs using the same tank and with the initial height of liquid set to be the same for all trials.

The tank used in these experiments had an inside diameter of 29.21 cm and a height of 86.40 cm. It was filled to 81.30 cm and then drained. The position of the free surface was recorded at 2.54 cm intervals. The exit orifice diameters used were 0.533, 0.668, 0.945, and 1.087 cm, corresponding to area ratios, A_t/A_0, of 3003, 1912, 955, and 722, respectively. The recorded total drain times, t_d, corresponding to these were 1223, 767, 403, and 288 s, respectively.

IV. RESULTS AND DISCUSSION

When the instantaneous heights of the free surface of water were plotted against time, they yielded the tank's draining pattern for the selected diameter of the exit orifice. The volume of water in the tank at any time is a linear function of the height of water in the tank because its cross-section is constant. Therefore, the volume of liquid remaining in the tank, or that of the liquid flowing out of it, could be calculated from the height of the free surface. Indeed, the ratio of
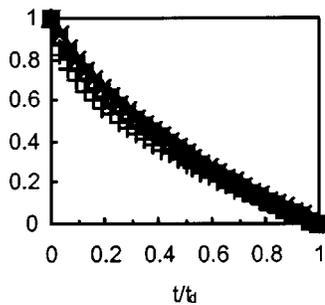
Fig. 2. Fractional height of the free surface of the liquid, h/h_0, as a function of the ratio of elapsed draining time to the emptying time, t/t_d, for values of the area ratio, A_t/A_0, of 3003 (open square), 1912 (open circle), 955 (open triangle), and 722 (solid cross) compared with the theoretical predictions of Eq. (3a) (plus).

Fig. 4. Calculated scaled height, h/h_0, as a function of the scaled time, t/t_0, for the free surface of the liquid (plus), and calculated scaled height, h_p/h_0, as a function of scaled time, t/t_f, for a free-falling particle (open circle).

heights, h/h_0, is equal to the ratio of the instantaneous volume of fluid that remains in the tank to the original volume of fluid in the tank when draining started.

The expressions derived above were compared to the corresponding results obtained experimentally. The variation of the height of the free surface of liquid with time is predicted to be parabolic in Eq. (3a). This result is compared to our experimental data in Fig. 2. Similarly, when the ratio between the cross-sectional area of the tank and that of the draining orifice is much larger than unity, inviscid-flow theory predicts that draining will be slow and that the time to empty the tank will vary linearly with that ratio. This result is given in Eq. (4) and is compared with experimental data in Fig. 3. In both cases, discrepancies between theory and experimental data were computed at each point and assessed. For the height of the free surface, discrepancies ranged from 0% to 14%, with an average value of 8.2%. For the total draining time, t_d, they ranged from 0.5% to 3% with an average value of 1.5%. It can be seen, therefore, that inviscid theory predicts the slow draining of a large tank reasonably well.

The forms of the expressions for $h(t)$ given in Eq. (3a), and for $h_p(t)$ given in Eq. (5), indicate several contrasting features between the motion of the free surface and that of a free-falling particle. These features are physically instructive because they help clarify the differences between the two behaviors.

(1) Unlike the free-falling particle, which is accelerated uniformly downward by gravity with a constant acceleration g, the falling free surface is uniformly decelerated in its
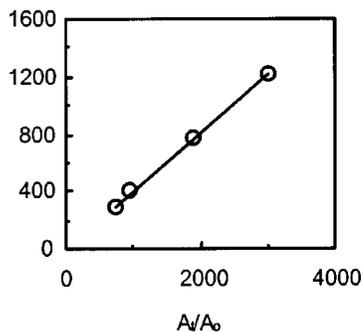
Fig. 3. Experimental values of the total time required to empty the tank, t_d, as a function of the area ratio A_t/A_0 (open circle) compared with the predictions of Eq. (4) (solid line).
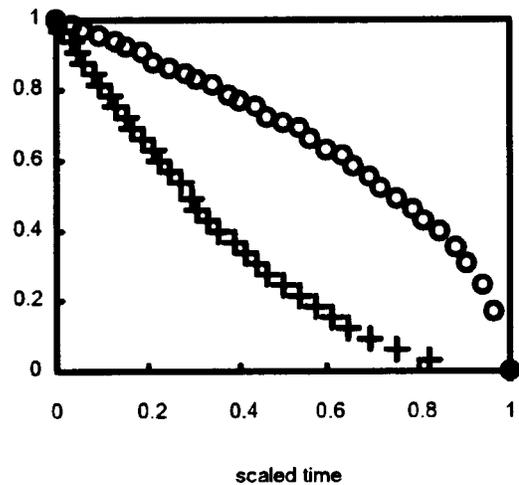
downward movement. The magnitude of the deceleration is given by Eq. (10); it is a small fraction of the acceleration of gravity, the fraction being determined by the area ratio, A_t/A_0. Figure 4 compares the motion of the free-falling particle in the absence of air resistance, as given in Eq. (5), to the downward movement of the free surface of a large tank that is being emptied slowly, as given by Eq. (3a).

(2) Unlike Eq. (7) for the free-falling particle that is released from rest, Eq. (3b) indicates that the initial velocity of the free surface is not zero. Indeed, by combining Eqs. (3b) and (4), it can be seen that the velocity of the free surface at $t=0$ is given by

$$ \nu(0) = \frac{\nu_f}{\sqrt{(A_t/A_0)^2 - 1]}}. \tag{11} $$

Equation (11) predicts a velocity that cannot be zero, while Eq. (3b) makes it possible to determine that it is twice as large as the average velocity of the draining process. This implies a rapid change in the velocity of the free surface, and, perhaps, even a sudden jump at the beginning of draining. Mathematically, this comes from the nature of Eq. (2), the simplified equation that was used to determine the solution in this application. It is of first order, and therefore the first derivative, which represents the velocity in this case, cannot be specified as an initial condition. Although surprising at first, the result indicated by Eq. (11) is consistent with the derivation of Eq. (1), which assumes that the tank is draining when analysis starts. Since the fluid is incompressible, the conservation of mass implies that the free surface of the liquid must be moving downward while draining is in effect. Accordingly, an impulsive start of the draining process is not modeled by Eq. (1).

(3) The downward motion of the free surface is much slower than that of a free-falling particle. One expects the area ratio, A_t/A_0, to be much larger than unity because the exit area, A_0, is ordinarily much less than the cross-sectional area of the tank, A_t. This ratio introduces an apparent acceleration of gravity g_m, given by Eq. (10), that is considerably smaller than the actual acceleration of gravity. Consequently, the time to drain the tank is much larger than the time it

would take a particle to fall freely from rest through a vertical distance h_0 equal to the original height of fluid at the start of the draining process.

(4) The distribution of mechanical energy during motion can also be used to explain the differences in the behaviors. In the case of a particle that is falling freely in the absence of air resistance, gravity is the only force that acts on it; because gravity is a conservative force, the total mechanical energy of the particle is conserved at all times. Since it consists of only kinetic energy and gravitational potential energy, the total mechanical energy is distributed between these two forms during motion. Taking the ratio between the instantaneous kinetic and gravitational potential energies for the falling particle, one obtains

$$R_f = \left(\frac{E_k}{E_p} \right)_f = \frac{(t/t_f)^2}{1-(t/t_f)^2}, \tag{12}$$

where E_k represents the kinetic energy, E_p the potential energy, and R_f their ratio. This ratio varies with time and, as expected, it increases during the fall because potential energy is continually converted into kinetic energy.

For a fluid particle on the free surface of the draining liquid, the situation is quite different. Gravity acts on it, but it is also in contact with the adjacent fluid. Its mechanical energy can be stored in three distinct forms: pressure, kinetic energy, and gravitational potential energy. The pressure that acts on it is the ambient atmospheric pressure because the tank is open. It is conventional to use the energy associated with atmospheric pressure as a reference. In that case, the total mechanical energy of this particle consists only of the sum of its kinetic and gravitational potential energies; however, when one computes the ratio between the two, as was done in Eq. (12) for the falling particle, one finds that the energy ratio for a particle on the liquid surface, R_s, is independent of time and given by

$$R_s = \left(\frac{E_k}{E_p} \right)_s = \frac{1}{(A_t/A_0)^2 - 1}. \tag{13}$$

Indeed, it is the same as the ratio obtained by dividing the acceleration of the free surface, given in Eq. (10), by the local acceleration of gravity. In the conventional terminology of fluid mechanics, the energy ratio expressed in Eq. (13) is proportional to the square of the Froude number. The slow draining of a large tank under gravity is, therefore, a process that maintains the Froude number[5] constant. The fact that this ratio does not vary with time can be explained in the following way. Draining causes the free surface to fall and, as before, potential energy is continually converted into kinetic energy. However, in this case, the kinetic energy generated by this conversion does not stay in the tank; it is carried out by the exiting mass of fluid. Therefore, both forms of energy decrease continually within the tank. If the draining process is slow enough, the free surface will decelerate slowly and uniformly, as described by Eq. (3c), and, as expected, Eq. (13) indicates that the kinetic energy of particles on the free surface will be very small compared to their potential energy.

V. CONCLUSION

The lab exercise discussed here considers the slow draining of a large tank under gravity. When the draining is modeled assuming an inviscid fluid in irrotational motion, theory predicts draining patterns and total draining times that are in good agreement with experiment. However, in our observations, the experiment is successful only when the exit orifices are small. Exit orifices for which data are reported here are such that ratios of the area of the tank to the area of the orifice were greater than or equal to 722. For much smaller area ratios, the acceleration of the fluid particles can no longer be assumed constant and negligible compared to that of gravity, and the quasisteady approximation is no longer valid. Indeed, the rate of fall of the free surface is so rapid that it is impractical to keep track of its location and to record the elapsed time with a stopwatch for more than one or two data points. In that case, computer data-acquisition systems have to be used. Although our experiments could not confirm it, it is important, nevertheless, to note that a theoretical estimate found in the literature indicates that the quasisteady approximation would hold for area ratios as low as 100.[3]

Although the slow draining of a large tank is a common problem in textbooks of fluid mechanics,[3–6] the author is not aware of experiments that show students that approximations used to solve it yield realistic results when tested in the laboratory. This exercise was used in our lab to fill this void. The apparatus that is needed is easy to build, and the experimental procedure is quite simple. The experiment can be used in introductory mechanics classes to illustrate uniformly decelerated motion that is caused by gravity. It can also be used to demonstrate that viscosity can be neglected in special circumstances, thereby justifying the use of inviscid flow models to approximate the behavior of real flows without recourse to advanced mathematical arguments about the behavior of viscous boundary layers.[4] The experiment can also be used to illustrate the difference between the downward motion of the free surface of a liquid during draining and the free fall of a solid particle, thereby motivating a discussion of the differences between the mechanics of fluids and the mechanics of solids. We have used this simple experiment for all these purposes over the years and our students have enjoyed learning mechanics from it.

[a] Electronic mail: libii@engr.ipfw.edu

[1] W. R. Debler, *Fluid Mechanics Fundamentals* (Prentice–Hall, Englewood Cliffs, NJ, 1990), pp. 225–227.

[2] J. Njock Libii and S. O. Faseyitan, "Data acquisition systems in the fluid mechanics laboratory: Draining of a tank," *Proceedings of the National Conference and Exposition of the American Society for Engineering Education (ASEE)*, Milwaukee, WI, Session 1426, June 1997.

[3] R. H. Sabersky, A. J. Acosta, and E. G. Hauptmann, *Fluid Flow: A First Course in Fluid Mechanics*, 5th ed. (Macmillan, New York, 1971), pp. 68–72.

[4] G. K. Batchelor, *An Introduction to Fluid Mechanics* (Cambridge University Press, Cambridge, 1994), pp. 378–392 and 511–517.

[5] T. E. Faber, *Fluid Dynamics for Physicists* (Cambridge University Press, Cambridge, 1995), pp. 37–46, 150–155, 186–188, and 222–225.

[6] J. W. Daily and D. R. F. Harleman, *Fluid Dynamics* (Addison-Wesley, Reading, MA, 1966), pp. 129–133.

A basic lock-in amplifier experiment for the undergraduate laboratory

K. G. Libbrecht,[a)] E. D. Black, and C. M. Hirata
Norman Bridge Laboratory of Physics, California Institute of Technology 264-33, Pasadena, California 91125

We describe a basic experiment for the undergraduate laboratory that demonstrates aspects of both the science and the art of precision electronic measurements. The essence of the experiment is to measure the resistance of a small length of brass wire to high accuracy using a simple voltage divider and a lock-in amplifier. By performing the measurement at different frequencies and different drive currents, one observes various random noise sources and systematic measurement effects. © *2003 American Association of Physics Teachers.*
[DOI: 10.1119/1.1579497]

I. INTRODUCTION

Precision electronic measurements are ubiquitous in modern physics. Experimental physicists are frequently faced with the challenge of measuring extremely small electronic signals from any number of sources. Given the widespread use of precision measurement techniques, we feel some obligation to teach at least some of the tools and tricks of this trade. We present here an undergraduate laboratory experiment that describes how the lock-in amplifier can be used to make precision measurements. The lock-in is an extremely versatile measurement tool, and the ideas behind lock-in detection are often used in experimental physics. Our experiment is relatively simple, inexpensive, and robust. Furthermore, it is a hands-on experiment, in which the student is guided through different aspects of the measurement process.

The focus of this experiment is simply to measure the resistance of a short length of brass wire. The resistance of our sample is about 80 mΩ, small enough that a typical hand-held digital multimeter is not up to the task. With a lock-in, however, the absolute resistance can be measured to within a fraction of a percent fairly easily. We like to point out that although measuring the resistance of a piece of wire is hardly cutting-edge physics, measuring the resistance of a nanotube, nanocontact, or some other small object is. For example, one can imagine that the wire would actually be 20 nm in diameter and 100 nm long, chilled to 50 mK, and be located at the bottom of an expensive cryostat. Given a maximum allowable current density of, say, 1 A/cm^2, we might be restricted to using only a few pA in our nanoscale experiment. We do the experiment with a simple wire described here because it is cheaper and it is nearly indestructible. Additionally, the wire measurement demonstrates nicely many noise sources and systematic errors that are often associated with precision electronic measurements. In addition to its intrinsic value, the experiment serves as a prerequisite for more advanced experiments that require lock-in detection.

II. BACKGROUND: LOCK-IN MEASUREMENT TECHNIQUES

We first describe the basic measurement techniques used for lock-in detection and signal measurement.[1–3] A lock-in amplifier is typically used when one has a small signal buried in noise. Consider an experiment in which we wish to measure the response of a system to some stimulus, and we know that the response is very weak. Furthermore, the output of the system, which is typically converted to an electronic signal, contains a lot of electronic noise that we cannot get rid of. Put in terms of voltages, our output signal looks like

$$V_{\text{signal}}(t) = V_0 + V_{\text{noise}}(t),$$

where V_0 is the response of the system we want to measure—here assumed to be constant in time—and $V_{\text{noise}}(t)$ is noise.

How we respond to this situation depends to some degree on the character of the noise $V_{\text{noise}}(t)$. In some cases the noise we are faced with is pure white noise, also called Gaussian noise. For this type of noise, $V_{\text{noise}}(t)$ fluctuates randomly and rapidly with time in such a way that the statistics of the noise are independent of time, and each value of $V_{\text{noise}}(t)$ is completely uncorrelated with $V_{\text{noise}}(t')$, provided that $|t-t'|$ is greater than some correlation time τ. A typical picture of white noise as a function of time is shown in Fig. 1. The power spectrum of white noise is independent of frequency up to frequencies $f \approx \tau^{-1}$; at higher frequencies the noise power typically goes to zero. With pure white noise our best recourse is to simply average the output signal with respect to time. White noise has zero expectation value, that is, $\langle V_{\text{noise}} \rangle = 0$, and by time-averaging we obtain $\langle V_{\text{signal}}(t) \rangle = \langle V_0 + V_{\text{noise}}(t) \rangle = \langle V_0 \rangle + \langle V_{\text{noise}}(t) \rangle \to V_0$, so we will get the answer we seek to high accuracy if we average for a long enough time.

In the real world, however, noise is seldom white. Amplifiers and other noise-generating elements often drift slowly with time. Over short periods the output of a typical amplifier will drift a small amount, and over long times it will drift a larger amount. Some of this comes from environmental effects—temperature drifts in the lab, creep in materials, etc., but some is intrinsic to many electronic devices. Detailed studies of many different types of electronic noise have shown that the frequency spectrum of these kinds of noise sources is often approximately proportional to $1/f$, where f is the frequency. Many electronic devices exhibit this "$1/f$ noise" even at very low frequencies. After much study there is still considerable debate over just what causes $1/f$ noise in many devices, but it certainly exists and is almost ubiquitous in amplifiers and other analog electronic devices. Figure 1 shows some typical $1/f$ noise in comparison with white noise.

In addition to white noise and $1/f$ noise, most detectors also provide some dc offsets to go along with whatever sig-
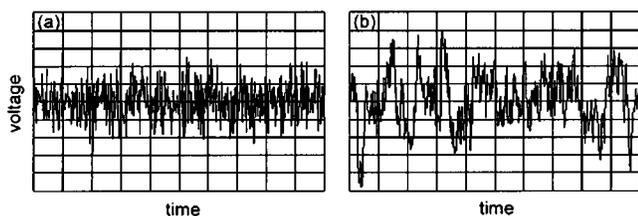
Fig. 1. The left panel (a) shows a signal as a function of time that is dominated by white noise, also called Gaussian noise. White noise has zero expectation value and averages to zero with time. The right panel (b) shows a signal dominated by $1/f$ noise, which is commonly seen in physics experiments. $1/f$ noise can be thought of as containing low-frequency drifts which do not average to zero with time (simulated noise plots from Milotti—Ref. 4).

nal one would like to measure. Including these terms, we see that a somewhat more realistic picture for the signal voltage would be

$$V_{\text{signal}}(t) = V_0 + V_{\text{offset}} + V_{\text{white noise}}(t) + V_{1/f\ \text{noise}}(t).$$

Even if we could remove V_{offset}, at low enough frequencies the noise will still be dominated by $1/f$ noise, and then a simple time-average is not going to work very well. A long time average will reduce the high-frequency noise contributions, but the longer we average, the more the low-frequency drifts inherent in $1/f$ noise will contaminate the signal. Once we are dominated by $1/f$ noise or voltage offsets, signal averaging will not be an effective way to improve our determination of V_0.

The situation is improved if we can control the signal voltage V_0. A particularly powerful trick is to chop the signal on and off at some high frequency and take the difference $V_{\text{on}} - V_{\text{off}}$. It is easy to see that any voltage offsets disappear from this difference voltage, and low-frequency drifts make little contribution as well; only higher-frequency noise contributes to the difference signal. If we can also average the difference signal over time, then we will be left with only a noise contribution at the chopping frequency. If the signal voltage is being digitized as a function of time, then it is a simple matter to perform the difference-and-average procedure in software; one just has to include a data flag to keep track of when the signal is on and when it is off. But another route is to use a lock-in amplifier to perform this task. A lock-in is a general purpose piece of laboratory equipment that can be adapted very quickly to different experiments.

Most modern lock-in amplifiers combine analog and digital electronics techniques. The input signal is first amplified and possibly filtered to remove noise above and below the reference frequency, and the resulting signal is then digitized. Lock-in amplifiers typically include a robust, well-behaved, low-noise preamplifier together with a set of electronic filters into which the signal is fed. Sometimes the signal filtering is done with analog electronic filters, and sometimes it is done digitally; the method depends on the particular lock-in used, but it is usually transparent to the user.

In addition to the signal input, one also needs to provide a reference input, which contains a waveform with a strong component at the frequency at which you are modulating the signal. The lock-in electronics then ''locks'' onto this reference signal and thus determines the operating frequency. A good lock-in can often extract a stable reference signal from a weak reference input, but more typically one presents the

lock-in with a square wave of several-volt amplitude that provides an unmistakable reference. Note that the reference signal contains not only a frequency but also a phase, and the latter is often very relevant to a given experiment. (The reference amplitude is irrelevant in principle.)

With a locked reference and a pre-processed input signal, the lock-in then manipulates the signals digitally to produce the desired output. Typically, the reference signal is converted into a sine wave with some adjustable phase, then multiplied by the signal input, and finally averaged to form

$$V_{\text{out}} = \langle V_{\text{signal}}(t)\cos(\omega t + \varphi) \rangle, \tag{1}$$

where the average is a running time average. This procedure picks out one Fourier component of the input signal $V_{\text{signal}}(t)$. If the signal we wish to measure is chopped, then the lock-in will pick out the first Fourier component of the square wave. In the experiment described below, our signal is sinusoidal in nature. Note that the exact method for generating V_{out}, particularly the way the time average is done, varies among lock-in amplifiers, so the expression above is only accurate up to a constant of order unity. Needless to say, these details are provided in the lock-in manual, although it is straightforward to send in a known signal to measure the proportionality constant directly.

A dual-phase lock-in, which is especially useful for some experiments, produces two outputs, the *in-phase* and *quadrature* outputs, given by

$$V_X = \langle V_{\text{signal}}(t)\cos(\omega t + \varphi) \rangle$$

and

$$V_Y = \langle V_{\text{signal}}(t)\sin(\omega t + \varphi) \rangle,$$

respectively, where φ is a parameter that one sets on the front panel of the lock-in. The lock-in can also be set to convert these signals digitally to amplitude, V_R, and phase, Φ, given, respectively, by

$$V_R = (V_X^2 + V_Y^2)^{1/2}$$

and

$$\Phi = \tan^{-1}(V_Y/V_X).$$

Both representations are useful, of course, depending on what kind of signal is being examined.

To see what a flexible instrument the lock-in amplifier is, consider the experiment shown in Fig. 2. Here the goal is to observe fluorescence from a sample illuminated by a laser. The laser beam is chopped using a mechanical chopping wheel, thus causing the fluorescence to turn on and off at the chopping frequency. The first thing you gain by using a lock-in for this experiment is flexibility. The lock-in has a very low-noise input amplifier, and the sensitivity can be adjusted over many orders of magnitude. Thus just about any input signal can be seen with a lock-in—this is very useful when one is frequently changing samples or laser parameters.

The second thing you gain is some freedom from worrying about ambient light getting into your detector. With the chopper working at 1 kHz or so, the lock-in can almost completely reject the dc and 60/120-Hz signals coming from ambient lights, provided these sources don't swamp either the detector or the lock-in (since both will have limited dynamic range). Finally, problems with voltage offsets and $1/f$ noise in the detector are also minimized using a lock-in.
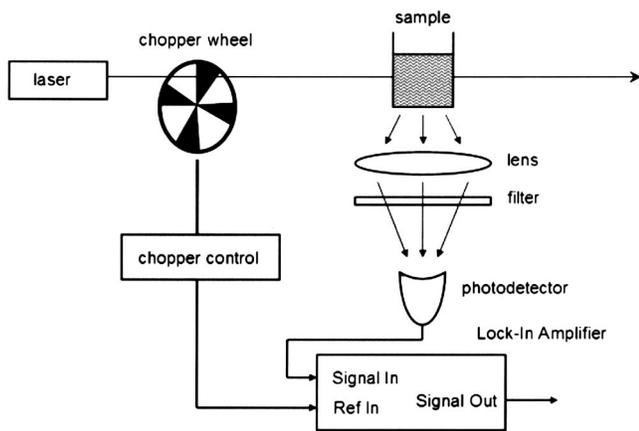
Fig. 2. A typical lock-in amplifier application in which one measures the fluorescence from a sample that is illuminated by a chopped laser beam—Ref. 5.

A popular lock-in demonstration experiment, shown in Fig. 3, is to modulate an LED using a simple square wave, say at 1 kHz, and examine the light output using a photodiode. With the LED close to the photodiode the signal can be seen clearly on an oscilloscope, and thus can be measured directly. With larger separations the photodiode signal becomes much weaker, to the point that it cannot be seen at all on the oscilloscope trace. With the lock-in detector, however, the signal remains strong at the lock-in output even after the photodiode signal appears to be swamped with noise from the ambient lighting.[1]

III. MORE BACKGROUND: NOISE SPECTRAL DENSITY

For any physically meaningful noise we can define a new "smoothed" noise function $V_{\text{noise},\tau}(t)$ that is a running time-average of the noise

$$V_{\text{noise},\tau}(t) = \frac{1}{\tau} \int_{t'=t}^{t'=t+\tau} V_{\text{noise}}(t')dt'.$$

For white noise we have that $\langle V_{\text{noise},\tau}(t) \rangle = 0$ and $\langle V_{\text{noise},\tau}(t)^2 \rangle^{1/2} \equiv \sigma_{\text{noise},\tau}$ is some constant (measured in units of volts). Physically this is a reasonable definition because we never actually measure the noise voltage at an instant in time, but rather we are always averaging over some short
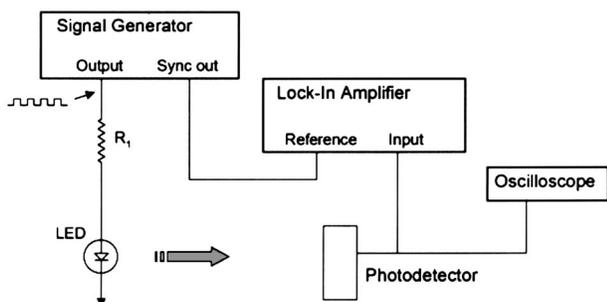
Fig. 3. A popular experiment to demonstrate how lock-in detection can recover a small signal buried in noise. When the LED is close to the photodetector, the signal is large and can be seen directly on the oscilloscope. When the LED is farther away, the signal is no longer visible on the oscilloscope, but is easily detected with the lock-in.

time τ. What we see plotted in Fig. 1 is not $V_{\text{noise}}(t)$, but rather $V_{\text{noise},\tau}(t)$. Naturally $V_{\text{noise},\tau}(t)$ depends on the averaging time τ, the longer the averaging time τ, the smaller $\sigma_{\text{noise},\tau}$ and $V_{\text{noise},\tau}(t)$ will be, and for white noise $\sigma_{\text{noise},\tau} \sim \tau^{-1/2}$.[6] We see that the averaging time τ is effectively equivalent to the noise correlation time mentioned above.

In the same way that measuring noise in the time domain always involves some averaging time τ, measuring the noise power spectrum always involves an average over a range of frequencies, called the measurement *bandwidth* (typically stated in Hz). If we compute the noise power spectrum using measurements over a finite time T_{ave}, then for white noise we find

$$\tilde{P}_{\text{noise},B}(f) = \left| \frac{1}{T_{\text{ave}}} \int V_{\text{noise}}(t)e^{i2\pi ft}dt \right|^2 \tag{2}$$

and

$$\langle \tilde{P}_{\text{noise},B}(f) \rangle = \frac{1}{T_{\text{ave}}^2} \left| \sum_{j=1}^{j=N=T_{\text{ave}}/\tau} \sigma_{\text{noise},\tau}(t_j)e^{i2\pi ft}\tau \right|^2$$

$$= \frac{1}{T_{\text{ave}}^2} N\sigma_{\text{noise},\tau}^2 \tau^2 = \frac{\sigma_{\text{noise},\tau}^2 \tau}{T_{\text{ave}}} = \sigma_{\text{noise},\tau}^2 \tau B,$$

where $B = 1/T_{\text{ave}}$ is the measurement bandwidth. The sum was evaluated knowing that the noise is uncorrelated over times greater than τ. Put another way, $V_{\text{noise}}(t)$ exhibits no long-range correlations, hence on long time scales the integral undergoes a random walk with a mean-squared value proportional to T_{ave}.

Since $\sigma_{\text{noise},\tau} \sim \tau^{-1/2}$ we see that $\langle \tilde{P}_{\text{noise},B}(f) \rangle$ is equal to some constant times the bandwidth B. We therefore define the bandwidth-independent *power spectral density*

$$S(f) = \lim_{T_{\text{ave}} \to \infty} \frac{1}{T_{\text{ave}}} \left| \int V_{\text{noise}}(t)e^{i2\pi ft}dt \right|^2$$

$$= \tilde{P}_{\text{noise},B}(f)/B.$$

We see that $S(f)$ is a well-defined function that depends on the intrinsic noise in the system as a function of frequency. $S(f)^{1/2}$ has the dimensions of $V/\sqrt{\text{Hz}}$ (called "volts per root hertz"), and this function is typically all one needs to know about the random noise in a signal. For pure white noise $S(f)^{1/2}$ is equal to a constant, while for $1/f$ noise $S(f)^{1/2} \sim 1/f$.

By comparing Eqs. (1) and (2) we see that $[\tilde{P}_{\text{noise},B}(f)]^{1/2}$ is precisely what the lock-in amplifier measures in the absence of any signal. Thus the fluctuations in the lock-in output V_{out} will be proportional to the power spectral density at the reference frequency, $S(f)^{1/2}$, times $B^{1/2}$, the square root of the bandwidth of the measurement. Note that $B = \beta/T_{\text{filter}}$ is the equivalent noise bandwidth when using a lock-in, where T_{filter} is the averaging time indicated by the lock-in, and β depends on how the signal averaging is performed (which is described in detail in the manual). Thus we see that the noise in a lock-in measurement will go like $T_{\text{filter}}^{-1/2}$, as we would expect.

One source of noise in our measurement, which the manufacturer has worked hard to reduce, is the input amplifiers inside the lock-in. For example, our lock-in manual states the input noise is no more than $6 \text{ nV}/\sqrt{\text{Hz}}$ at 1 kHz. Thus if our
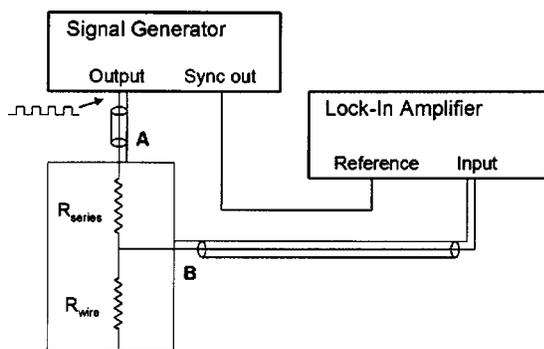
Fig. 4. The circuit used to measure the resistance R_{wire}. The two resistors are soldered together and placed into a small box; the rest of the connections are made using coaxial cables.

Fig. 5. A measurement of R_{wire} as a function of the signal generator frequency with a large fixed input voltage. Specifically, $V_{A,set}$ was a 1-V sine wave, and the lock-in time constant was 3 s. R_{wire} was determined using either the total signal amplitude $V_{B,R}$ or the in-phase component $V_{B,X}$. This graph demonstrates systematic effects in the measurement that arise from capacitive effects. These effects are reduced by using the in-phase signal $V_{B,X}$, but they are not eliminated.

reference is at 1 kHz and we short the lock-in input with some small resistor (so the input signal is zero), then the signal we measure would have an effective noise of $6\ \mathrm{nV}/\sqrt{\mathrm{Hz}}$. Therefore, if we integrate for 10 s, the output display should display rms fluctuations of about $6/\sqrt{10}$ nV ≈ 2 nV.

Resistors can introduce noise from thermal fluctuations into a measurement. This is called resistor *thermal noise*, or *Johnson noise*, and the rms amplitude of the thermal noise voltage is given by

$$V_{\mathrm{rms,thermal}} = \sqrt{4kTRB} \quad (\mathrm{V}),$$

or in terms of spectral density

$$V_{\mathrm{rms,thermal}}(\text{spectral density}) = \sqrt{4kTR} \quad (\mathrm{V}/\sqrt{\mathrm{Hz}})$$

$$= 0.128 \sqrt{\frac{R}{1\Omega}} \quad (\mathrm{nV}/\sqrt{\mathrm{Hz}}),$$

where R is the resistance value and B is the bandwidth of measurement.

IV. MEASURING A RESISTOR

The objective of the first part of this lab is to measure the resistance of a short length of brass wire. Specifically, we use an unknown alloy wire with a length of 17 cm and a diameter of 0.4 mm that gives a resistance of about 80 mΩ. There are essentially two ways to measure the electrical resistance of any device—one can either send a known current through it and measure the resulting voltage across it, or apply a known voltage and measure the resulting current through it. In most cases, including our case, the former option is technically easier. We use the simple resistor divider circuit shown in Fig. 4 with $R_{series} = 1$ kΩ. The current in this case is $I = V_A/(R_{series} + R_{wire})$, and the voltages we need to measure are V_A and V_B. The wire resistance can then be computed as

$$R_{wire} = \frac{V_B}{V_A} R_{series} \left(1 + \frac{R_{wire}}{R_{series}} \right) \approx \frac{V_B}{V_A} R_{series},$$

where in our case the approximation is accurate to a part in 10^4. We see that our measurement of R_{wire} can be no more accurate than our knowledge of R_{series}, but since R_{series} is approximately 1 kΩ we can measure it fairly accurately with a simple digital multimeter.

For our experiment we use a Stanford Research Systems model SR830 DSP lock-in amplifier, and a Berkeley Nucleonics Corporation Model 625 signal generator is used to generate a sine-wave signal. The circuit configuration in Fig. 4 was used to measure V_B, and the signal generator was connected directly to the lock-in input to measure V_A. From these voltages R_{wire} was determined as a function of V_A and the signal generator frequency ν. [One important feature of the circuit that is not shown in Fig. 4 is a 4:1 voltage divider that was inserted between the signal generator sync output and the lock-in reference input. This divider reduced the level of the sync signal by a factor of 4 before it went into the lock-in amplifier. In principle, this divider should do nothing; however, before this divider was inserted (i.e., when the sync out was fed directly into the lock-in reference input) we found a small but significant offset in the lock-in reading. We do not understand the origin of this problem, but it appears to be due to cross-talk inside the lock-in amplifier. The divider seemed to eliminate this problem completely.]

We want to convey an important lesson: all precision measurements are limited by both random noise and systematic effects. Much of the art of experimental physics is dealing with these problems. To demonstrate the kinds of systematic errors that can be present, we first measure R_{wire} as a function of ν with the signal generator output set point, $V_{A,set}$ fixed. (Our signal generator is digital, so $V_{A,set}$ is a numerical input value; however, we always measure V_A directly using the lock-in.) We measure R_{wire} two ways: using the measured signal amplitude $V_{B,R}$, and using the in-phase component $V_{B,X}$ (recall the definition $V_R^2 = V_X^2 + V_Y^2$ given above). The lock-in phase is adjusted so that the direct measurement of V_A gives $V_Y = 0$; that way, we expect $V_{B,Y} = 0$ if our resistors have purely real impedances. (In our case the phase offset between the signal generator output and the sync out was measured to be 2.3°.)

The results of these measurements are shown in Fig. 5. Note that we used a large $V_{A,set}$ and a long time constant τ_0,
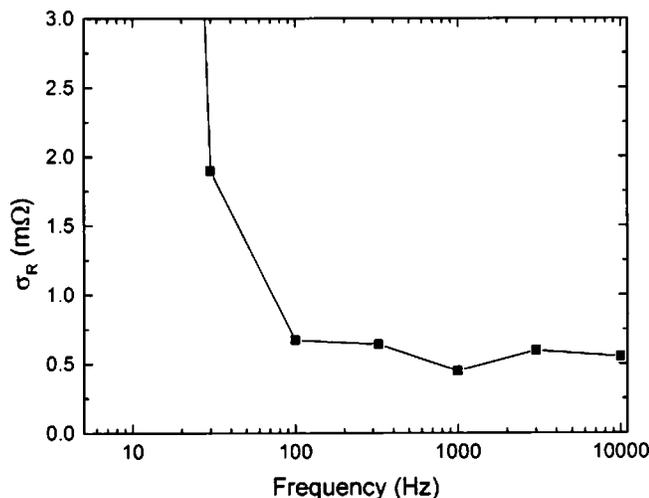
Fig. 6. The random noise in a single measurement of R_{wire} made with a small input voltage and a small lock-in time constant. Specifically, $V_{A,set}$ was a sine wave of 10-mV amplitude, and the measurement was made using the in-phase component $V_{B,X}$ and a lock-in time constant of 0.3 s. This demonstrates how the noise increases sharply when the measurement is done at low frequencies.

Fig. 7. Measurements of R_{wire} as a function of the input voltage V_A. The frequency is fixed at $\nu=1$ kHz. The measurement was made using $V_{B,X}$ data and a lock-in time constant of 0.3 s. Again we see how systematic errors dominate the uncertainty, particularly when the signal level is low.

so the random noise in these measurements is small. We first see that our measurements of R_{wire} based on $V_{B,R}$ are constant at low frequencies, but increase rapidly above about 3 kHz. The frequency dependence comes mainly from capacitive effects—the cable capacitance and the stray capacitance couple with the finite output impedance of the signal generator to produce a complex impedance. The interested student is invited to investigate these effects by changing cable lengths and by adding a small series resistor between the signal generator and R_{series} (thus changing the effective signal generator output impedance). The hands-on nature of this simple experiment makes this kind of investigation easy to perform although we don't require it as part of the lab. The main lesson from the graph in Fig. 5 is that the real circuit is not necessarily the same as the ideal circuit drawn in Fig. 4. The power of lock-in detection is that one can simply measure R_{wire} as a function of ν to see the magnitude of these systematic effects directly.

If the systematic effects were entirely capacitive, we would expect to obtain a more accurate measurement of R_{wire} using $V_{B,X}$, the in-phase component of V_B, because the capacitive impedances are purely complex. We see in Fig. 5 that this is indeed the case. Using $V_{B,X}$, one finds that the systematic errors become very large only above about 30 kHz, where they are a factor of 10 higher than what one obtains using $V_{B,R}$. At very high frequencies we see that the circuit in Fig. 4 no longer represents the real circuit well at all, so our determination of R_{wire} would have to proceed differently at high frequencies.

Another lesson we wish to convey in this lab is that random errors are also frequency dependent owing to $1/f$ noise and other effects. To demonstrate this we again measure R_{wire} as a function of frequency, but this time with a small $V_{A,set}$ and a shorter time constant τ_0. The random errors are estimated simply by recording 16 separate measurements of $V_{B,X}$, the measurements separated by several τ_0. The standard deviation σ_R was then determined from these 16 samples. The results are shown in Fig. 6. We see that σ_R is
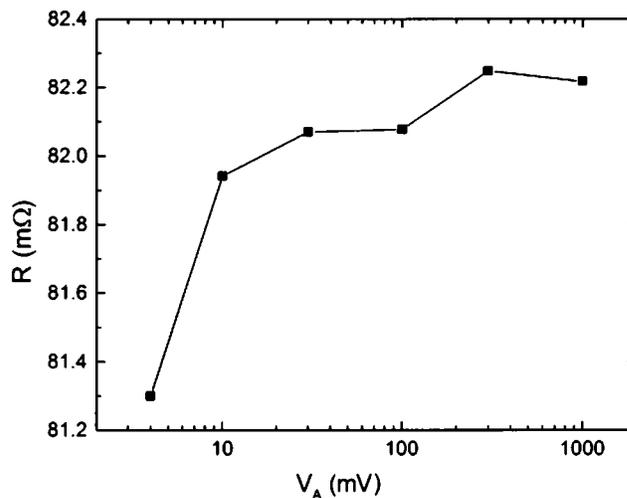
much higher at low frequencies, probably due to the intrinsic noise in the lock-in amplifier. The curious student is invited to compare these measurements with the noise specifications given in the lock-in manual. We note by comparing Figs. 5 and 6 that there is an optimal frequency for making measurements of R_{wire}. If ν is too high, systematic errors become problematic; if ν is too low, the random noise is greater. An interesting side point is that the measurement errors were huge at $\nu=300$ Hz when V_A was small, because of 60-Hz noise harmonics. This problem was eliminated by measuring at $\nu=325$ Hz instead of 300 Hz.

Next we ask students to determine just what R_{wire} really is, and how well it can be measured if we are restricted to passing only very small currents through the wire. To this end we measure R_{wire} as a function of $V_{A,set}$, with the frequency fixed at $\nu=1$ kHz. We use a long time constant to reduce the random fluctuations in V_B. The results are shown in Fig. 7. Again we see a systematic trend with V_A, which is probably due to some unexpected signal coupling, either in our circuit or in the lock-in itself. With $V_A=4$ mV we find that V_B is only 300 nV, so there are any number of stray voltage effects that could produce the necessary offset. The interested stu-
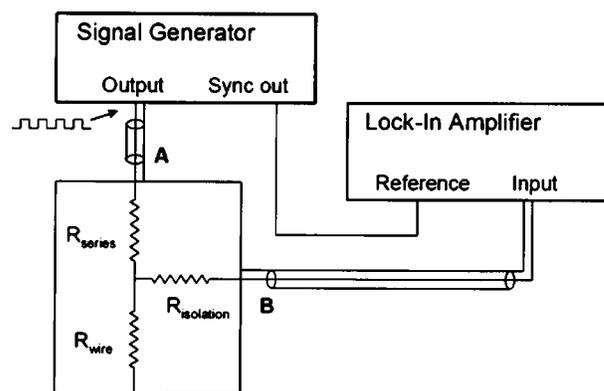
Fig. 8. A circuit schematic for measuring R_{wire} in the presence of an isolation resistor. By varying $R_{isolation}$ the Johnson noise can be measured.

dent is invited to try and track this down. In the end we see from Fig. 7 that $R_{wire} \approx 82.2 \pm 0.2$ mΩ, with the uncertainty coming mainly from systematic effects. An absolute accuracy of 0.25% is not too bad for such a small resistor, using such a simple circuit. This level of accuracy is sufficient to see the change in R_{wire} when it is warmed slightly, by cupping one's hands around the wire or by blowing on it slightly.

Finally, we use the circuit in Fig. 8 to demonstrate the effects of Johnson noise. This circuit is motivated by imagining that our sample is sitting at the bottom of a cryostat at 100 mK. In this case we cannot connect wires to it directly because of the heat load, and therefore $R_{isolation}$ cannot be made too small. By measuring σ_R again with different values for $R_{isolation}$, Johnson noise can be observed.

V. DISCUSSION

The purpose of this laboratory experiment is to introduce students to the science and art of precision electronic measurements. This hands-on lab demonstrates the concepts of lock-in detection, noise spectral density, and the trade-offs between random and systematic errors. We use the lab as a prerequisite for other labs requiring the use of lock-in detection for small-signal measurements. We believe this lab also reinforces the point that precision measurements can be tricky, hence varying whatever measurement parameters one can vary (in this case V_A and ν) is good experimental practice.

[a] Electronic mail: kgl@caltech.edu

[1] P. Horowitz and W. Hill, *The Art of Electronics* (Cambridge U.P., New York, 1989), 2nd ed., p. 1031.

[2] D. W. Preston and E. R. Dietz, *The Art of Experimental Physics* (Wiley, New York, 1991), p. 367.

[3] R. Wolfson, Am. J. Phys. **59**, 569 (1991).

[4] Simulated noise plots from Edoardo Milotti, at http://www.fisica.uniud.it/milotti/Research/loverf/loverf_noise.html (2002) (with permission).

[5] Graph adapted from http://www.chem.vt.edu/chem-ed/electronics/instrum/lock-in.html.

[6] D. T. Gillespie, Am. J. Phys. **64**, 225 (1996); **61**, 1077 (1993).